ISIJ International, Vol. 59 (2019), No. 5, pp. 889–894

Numerical Simulation on Interfacial Creep Generation for Shrink-fitted Bimetallic Roll

Hiromasa SAKAI, Nao-Aki NODA,* Yoshikazu SANO, Guowei ZHANG and Yasushi TAKASE

Dept. of Mechanical and Control Engineering, Kyushu Institute of Technology, 1-1 Sensui-cho, Tobata-ku, Kitakyushu-shi, 804-8550 Japan.

(*Received on November 8, 2018; accepted on December 28, 2018; originally published in Tetsu-to-Hagané, Vol. 105, 2019, No. 4, pp. 411–417*)

The bimetallic work rolls are widely used in the roughing stands of hot rolling stand mills. The rolls are classified into two types; one is a single-solid type, and the other is a shrink-fitted assembled type consisting of a sleeve and a shaft. Regarding the assembled rolls, the interfacial creep sometimes appears between the shaft and the shrink-fitted sleeve. This interfacial creep means the relative displacement on the interface between the sleeve and the shaft. This creep phenomenon often causes damage to the roll such as shaft breakage due to fretting cracks. Although to clarify this creep mechanism is an important issue, experimental simulation is very difficult to be conducted. Since few studies are available, in this paper, the interfacial creep phenomenon is simulated by using the elastic finite element method (FEM) analysis. Here, the roll rotation is replaced by the road shift on the fixed roll surface. It is found that the interface creep can be explained as the accumulation of the relative circumferential displacement along the interface.

KEY WORDS: shrink fitting; rolling roll; bimetallic roll; interfacial creep; sleeve; shaft.

1. Introduction

Among rolling rolls used in steel industries, sleeve assembly types were tried to be used and some of them were practically and successfully used by shrinkage-fitting shafts into a hollow cylinder. They have some advantages for back-up rolls having large trunk diameter exceeding 1 000 mm[1)] and also for rolling rolls for large H-section steel.[2,3)] Due to the abrasion and the surface roughening, the roll body is consumed in a short period; however, after reaching the threshold minimum diameter, the shaft can be reused in this shrink-fitted structures. Furthermore, the sleeve wear resistance can be improved independently without loosening the shaft ductility. On the other hand, this shrink-fitted structure has several peculiar problems such as residual bend deformation,[4)] fretting fatigue cracks at the sleeve end and sleeve fracture due to the circumferential sleeve slippage.[5,6)] The circumferential slippage sometimes occurs even though the resistance torque at the interface is larger than the motor torque.

Few studies are available for this circumferential slippage in rolling roll, but a similar phenomenon is known as interfacial creep in ball bearing attracting attention.[7–9)] An interfacial creep phenomenon in ball bearing in the opposite direction of the bearing rotation is regarded as the accumulation of elastic deformation.[7)] Although there are some similarities such as the sliding direction between the bearing and the sleeve assembly roll, no analytical studies are available to simulate this phenomenon and to discuss the generation mechanism by numerical analysis in the sleeve assembly type roll.

Therefore, in this study, we assume the creep phenomenon seen in rolling bearings as a factor of circumferential slippage in the sleeve assembly type rolling roll. Here, this creep phenomenon is defined as an interfacial creep. By this research, if we can clarify the creep generation mechanism, we can explain the circumferential slippage in the rolling roll. In the future, it is possible to design a sleeve assembly type rolling roll that can prevent circumferential slippage. Therefore, in this research, the interfacial creep of the sleeve is reproduced by numerical analysis using the finite element method, and its generation mechanism is quantitatively clarified.

2. Numerical Simulation for Interface Creep Appearing at Shrink-Fitted Surface

Figure 1 show schematic illustration of a sleeve assembly type roll used in four rolling mill during rolling. Figure 1(a) shows the central cross section view of rolling roll and Fig. 1(b) shows the axial section view of rolling roll. The sleeve roll in Fig. 1 is assembled with a shaft and a sleeve by shrink fitting. The sleeve is required to have different properties, that is, high abrasion resistance and high fracture toughness. Therefore, the composite sleeve is usually used consisting of the outer and inner layers. Then, the outer layer has high abrasion resistance made of high-speed steel or high chro-

* Corresponding author: E-mail: noda.naoaki844@mail.kyutech.jp
DOI: https://doi.org/10.2355/isijinternational.ISIJINT-2018-749

mium steel, and the inner layer has high ductility made of alloy steel. The loads on the roll are compressive force P from the backup roll to the sleeve, the rolling reaction force P_h and the frictional force S from the strip to the sleeve, the bending force P_b from the bearing to the shaft and torque T from the motor to the shaft. Sano reported a case of hot rolling,[10] and the load condition of this research was determined based on that case. Also, the target is the reference roll No. 5.[10] In addition, the analysis model shown in **Fig. 2** is a two-dimensional model, therefore the unit of force is per unit length. The rolling force P, the rolling reaction force P_h and the bending force P_b are in a balanced relationship, but under the load condition of the referenced roll,[10] the bending force is small on the order of three orders of magnitude, and the rolling force (= P × backup roll body length) and rolling reaction force (= P_h × strip width) are almost equal ($P \simeq P_h$). Therefore, the rolling reaction force from the backup roll to the sleeve and the rolling reaction force from the strip to the sleeve are equal ($P = P_h$), and in Fig. 2 and the following figures, both are expressed as the rolling reaction force P.

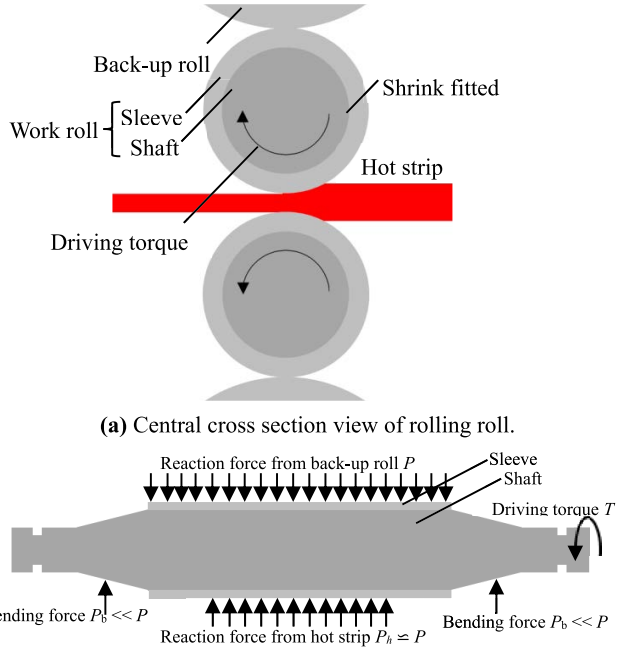

(a) Central cross section view of rolling roll.

(b) Axial section view of rolling roll.

Fig. 1. Schematic illustration for real hot strip rolling roll. (Online version in color.)

As shown in Fig. 2, the roll rotation is expressed by the load shifting on the fixed roll surface.[11,12] Figure 2(a) shows a two-dimensional model rotating. As shown in Fig. 2(b), by the discrete load shifting with a constant interval φ_0, the continuous roll rotation is expressed. Although the analysis results are depending on the load shift interval φ_0, the most suitable value of φ_0 is found out to reduce the computational time without loosening the computational accuracy.

Figure 3 illustrates two-dimensional numerical simulation model considered in this paper. Figure 3(a) shows the real loading shift equivalent to the actual roll rotation. Under stable rotation, the torque T from the motor should be balanced with the torque due to the friction force S from the strip as $T=SD/2$. The balanced torque T and the friction S promote the interfacial slippage. Figure 3(b) shows a simplified model assuming $T = 0$ and $S = 0$. Here, by putting a small rigid body region at the roll center, the displacement and rotation are fixed at the roll center. In Fig. 3(b), the interfacial creep can be described as the relative displacement along the interface. Furthermore, Fig. 3(c) shows a more simplified 2D model. By assuming the entire rigid shaft and the steel sleeve, the interfacial creep generation can be directly expressed from the interfacial displacement at the sleeve interface. At the shrink-fitted surface, the resistance torque against the roll rotation is always designed to be larger than the motor torque to prevent slippage.[5,6] In the following discussion, the shrink fitting ratio will be chosen to satisfy such conditions.

Table 1 shows the dimensions, mechanical properties and boundary conditions of the 2D roll model in Fig. 3(c). The roll is supposed to be subjected to the concentrated load P = 13 700 N/mm from the backup roll to the sleeve and also subjected to the reaction concentrated load P = 13 700 N/mm from the strip. In real rolls, distributed loads should be considered but the preliminary analysis shows that the effect of the distributed load on the displacement at the shrink-fitted surface is not very large. The shrink fitting ratio is defined as δ/d, where δ is the diameter difference between the inner diameter of the sleeve and the outer diameter of the shaft. Then, $\delta/d = 0.5 \times 10^{-3}$ is used with the coefficient of friction between the sleeve and the shaft $\mu = 0.3$.

In this research, the finite element method (hereinafter referred to as FEM) will be used to shrink-fitted roll for the numerical simulation of interfacial slippage. The FEM can be applied to such structures composed of different materials. Various applications of the finite element method have been seen, relatively easy to apply to composite materi-

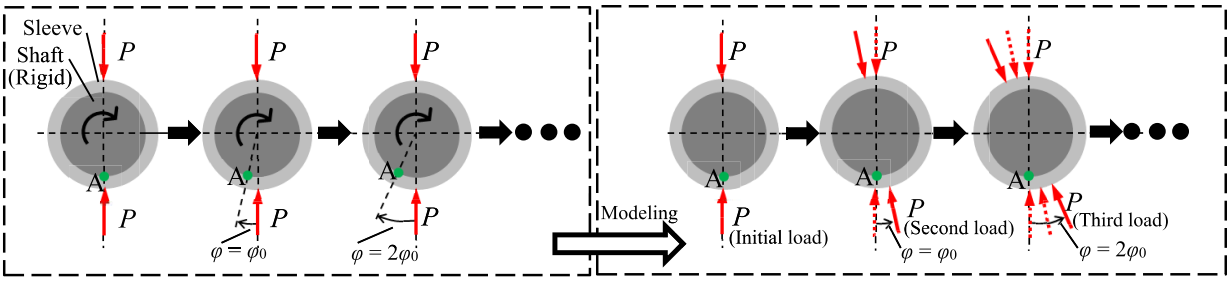

(a) Rotation of the real roll.

(b) Rotation of the roads in the modeling.

Fig. 2. The rotation of the roll replaced by the discrete shifted loads at interval of the load shift angle φ_0. (Online version in color.)

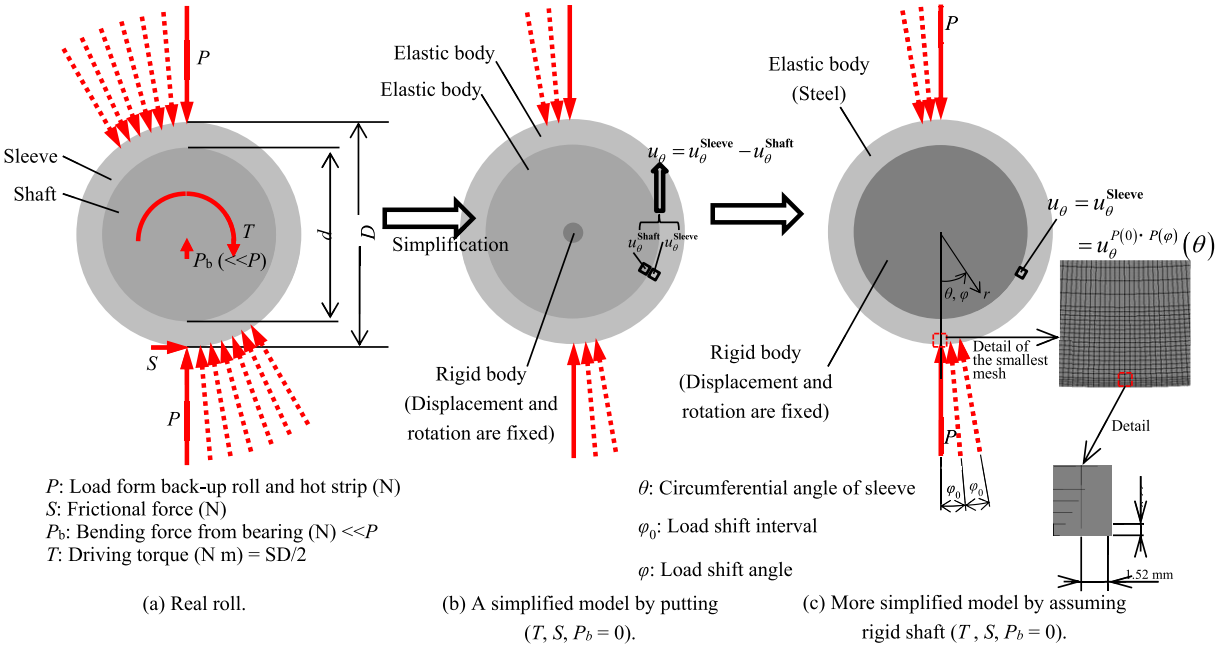

Fig. 3. Modeling of FEM 2D model. (Online version in color.)

Table 1. Dimensions, mechanical properties and boundary conditions of roll model.

Mechanical properties	Sleeve	Young's modulus of steel sleeve E	210 GPa
		Poisson's ratio of steel sheeve ν	0.28
	Shaft	Young's modulus of rigid shaft Es	∞
Roll size		Outer diameter of sleeve	700 mm
		Inner diameter sleeve d	560 mm
Shrink fitting		Shrink fitting ratio δ/d	0.5×10^{-3}
		Friction coefficient between sleeve and shaft μ	0.3
External force		Concentrated load per unit thickness P	13 270 N/mm Total: 1.327×10^7 N Rolled width: 1 000 mm
		Frictional force per unit thickness S	0 N m
		Motor torque per unit thickness T	0 N m
		Bending force from bearing P_b	0 N m

als,[13–16] accurate analysis for test specimens,[17] complicated 3D structure analysis like bolts and nuts[18] have be done, and a lot of general-purpose FEM software programs have been developed. In this study, Marc/Mentat 2012 general-purpose finite element analysis software is used and elastic contact analysis will be performed. Marc uses the complete Newton-Lapthorne method, and the contact analysis uses the direct constraint method[19] by using the tetrahedral plane strain first order element with the number of elements 46080.

3. Numerical Simulation Results for Interfacial Creep

The interfacial creep for the shrink-fitted surface can be expressed by the relative displacement in the circumferential direction between the sleeve and the shaft. As described in the previous section, since the rigid shaft modeling is assumed in this analysis, the interfacial relative displacement of the sleeve is equal to the interfacial absolute displacement of the sleeve. Therefore, the interfacial displacement in the circumferential direction of the sleeve $u_\theta^{P(0)\sim P(\varphi)}(\theta)$ is used for expressing the interfacial creep. **Figure 4** shows the definition of the interfacial displacement of the sleeve $u_\theta^{P(0)\sim P(\varphi)}(\theta)$ when the load $P(\varphi)$ shifts from $\varphi = 0$ to $\varphi = \varphi$ on the outer surface of the sleeve. Here, φ denotes the angle where the load is shifting and θ denotes the position where the displacement is evaluated. The load $P(\varphi)$ is defined as the pair of loads acting at $\varphi = \varphi$ and $\varphi = \varphi + \pi$. The notation $u_\theta^{P(0)\sim P(\varphi)}(\theta)$ means the displacement $u_\theta(\theta)$ at $\theta = \theta$ when the pair of loads are applied at $\varphi = 0$ to φ and $\varphi = \pi$ to $(\varphi + \pi)$.

Figure 5 shows the effect of the load shift angle φ_0 on the displacement of the point A. By comparing the result of $\varphi_0 = 0.25°$ corresponding to the minimum dimension of the element with the results of $\varphi_0 = 4°$, 8° and 12°, it is seen that the relative error between $\varphi_0 = 0.25°$ and $\varphi_0 = 4°$ is several percent or less (a few % in the range of Fig. 5), the load shift angle $\varphi_0 = 4°$ is adopted. In this analysis, the shaft is an rigid body and the rotation is restrained. Therefore, when the rotation of the roll is expressed by the load shifting

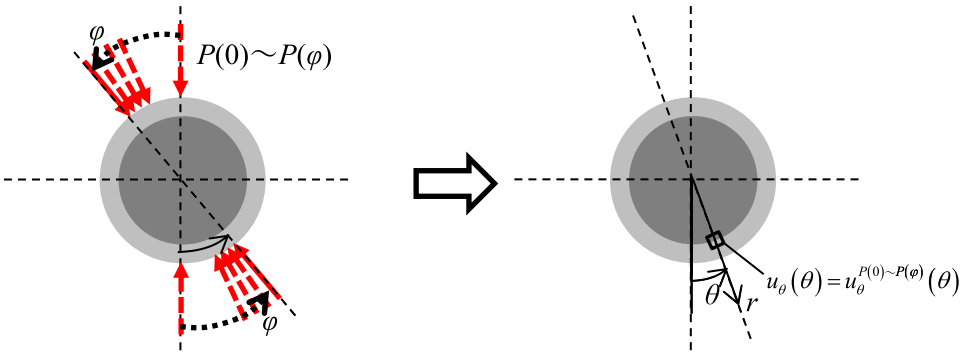

(a) Definition of $P(0)\sim P(\varphi)$meaning the pair of the loads shifting from $\varphi = 0$ to φ, and $\varphi = \pi$ to $(\pi + \varphi)$ as $P(0)\sim P(\varphi)$.

(b) Definition of the displacement $u_\theta^{P(0)\sim P(\varphi)}(\theta)$ meaning $u_\theta(\theta)$ due to $P(0)\sim P(\varphi)$.

Fig. 4. Definition of interfacial displacement $u_\theta^{P(0)\sim P(\pi)}(\theta)$ due to the shifted load $P(0)\sim P(\varphi)$. (Online version in color.)

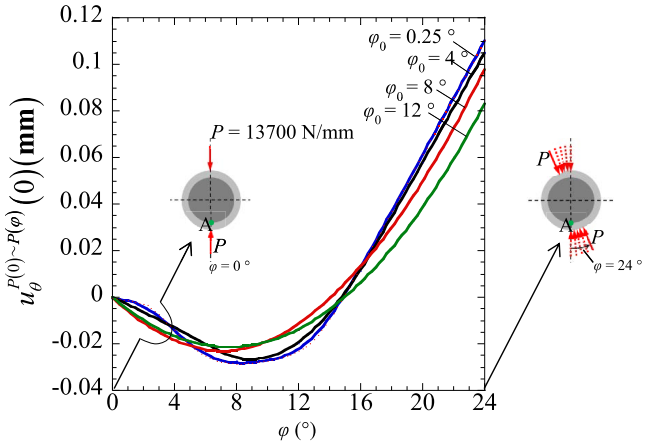

Fig. 5. Effect φ_0 on the displacement $u_{\theta,\text{ave.}}^{P(0)\sim P(\varphi)}(0)$ (Point A). (Online version in color.)

as shown in Fig. 2(b), there is no angular difference between the position of the load and the position where displacement occurs in the rigid body. Since the sleeve is an elastic body, an angular difference occurs between the position of the load and the position where displacement occurs in the elastic body. This means that the circumferential interfacial relative displacement of the rigid shaft surface and the the elastic sleeve surface is equal to the interfacial absolute displacement of the elastic sleeve surface.

Figure 6 shows the displacement distribution $u_\theta^{P(0)}(\theta)$ due to the load P(0) in Fig. 6(a) and the displacement distribution $u_\theta^{P(0)\sim P(\pi)}(\theta)$ due to the load shifting P(0) ~ P(π) and P(0) ~ P(2π) in Fig. 6(b). It is seen that in Fig. 6(a) the displacement is symmetric with respect to $\varphi = 0$ as can be expressed in Eq. (1).

$$-u_0^{P(0)}(-\theta) = u_0^{P(0)}(\theta) \quad \text{..... (1)}$$

Figure 6(b) shows the displacement distributions $u_\theta^{P(0)\sim P(\pi)}(\theta)$ and $u_\theta^{P(0)\sim P(2\pi)}(\theta)$, both of which do not have such symmetry anymore as shown in Eq. (2).

$$-u_\theta^{P(0)\sim P(2\pi)}(-\theta) \neq u_\theta^{P(0)\sim P(2\pi)}(\theta) \quad \text{..... (2)}$$

In Figs. 6(a) and 6(b) the average value of the displacements are also shown using notations $u_{\theta,\text{ave.}}^{P(0)}$ and $u_{\theta,\text{ave.}}^{P(0)\sim P(\varphi)}$. The average displacement is defined as Eq. (3).

$$u_{\theta,\text{ave.}}^{P(0)\sim P(\varphi)} = \frac{1}{2\pi}\int_0^{2\pi} u_\theta^{P(0)\sim P(\varphi)}(\theta)\,d\theta \quad \text{..... (3)}$$

When the initial load P is applied at $\varphi = 0$, the average displacement $u_{\theta,\text{ave.}}^{P(0)} = 0$ and $u_\theta^{P(0)}(\theta)$ having the symmetry. However, when the load is shifting from $\varphi = 0$ to $\varphi = \varphi$, the symmetry is lost and the average displacement $u_{\theta,\text{ave.}}^{P(0)\sim P(\varphi)} \neq 0$.

In order to clarify the relationship between the occurrence behavior of interfacial creep and the load shift angle φ, **Fig. 7** shows the relationship between the load shift angle φ and the average interface displacement $u_{\theta,\text{ave.}}^{P(0)\sim P(\varphi)}$. From Fig. 7, it can be seen that $u_{\theta,\text{ave.}}^{P(0)\sim P(\varphi)}$ increases with increasing the load shift angle φ. From Fig. 7, it may be concluded that the interface creep occur as soon as the load shifting starts.

4. Slippage Zone of Shrink-fitting Surface and Residual Displacement

In the previous section, we focused on the displacement of the sleeve interface to investigate the interfacial creep of the shrink-fitted roll. Form Fig. 6, the sleeve interface is moving in the circumferential direction due to the load shifting. From Fig. 7, the average displacement $u_{\theta,\text{ave.}}^{P(0)\sim P(\varphi)}$ increases with increasing the load shifting angle φ. To explain the reason why the average displacement increases, the residual displacement at the interface will be focused. The residual displacement is a kind of irreversible change since the interface displacement does not return to the state before the loading even though the external force is removed. If this residual displacement appears, the symmetry condition of the circumferential displacement no longer holds on the interface because of the load shifting. In other words, as a result of the residual displacement at each loading angle is accumulated, the average displacement increases with increasing the load shifting.

In the previous study,[4] Noda *et al.* have studied the relationship between slippage and residual deflection in axial direction for the back-up roll composed of the shrink-fitted sleeve and the shaft. They have indicated that the residual deflection is similar to the relative slippage between the sleeve and the shaft. From the stress distributions $\tau_{r\theta}$ and $\mu\sigma_r$ along the shrink-fitted surface, they have discussed the

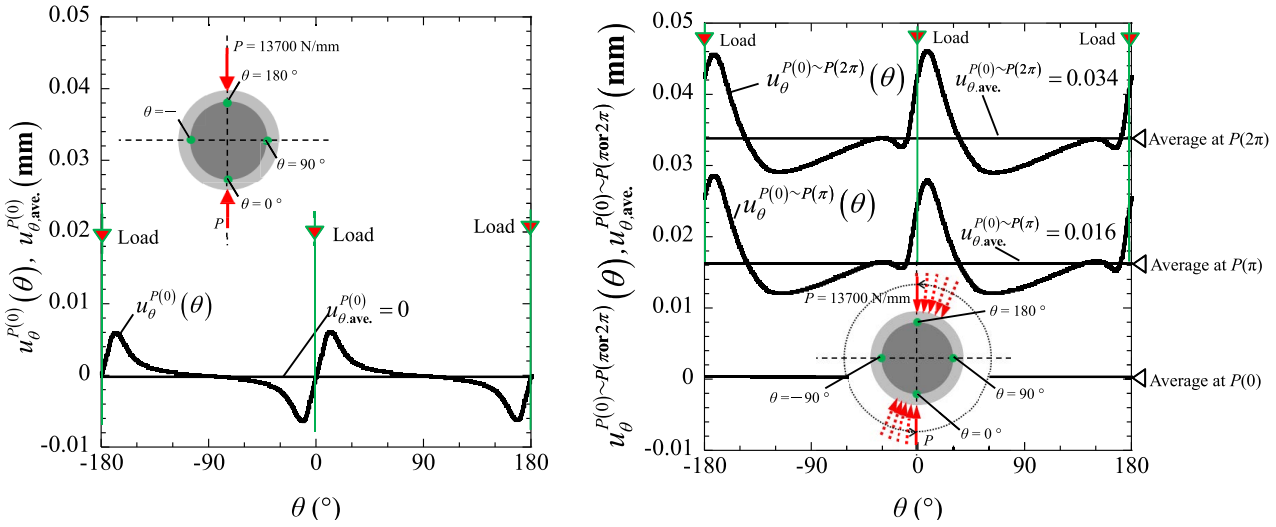

(a) Displacement due to the initial loading $P(0)$. (b) Displacement due to loading shift $P(0) \sim P(\pi)$ and $P(0) \sim P(2\pi)$.

Fig. 6. Displacement comparison between due to stationary load and shifted load. (Online version in color.)

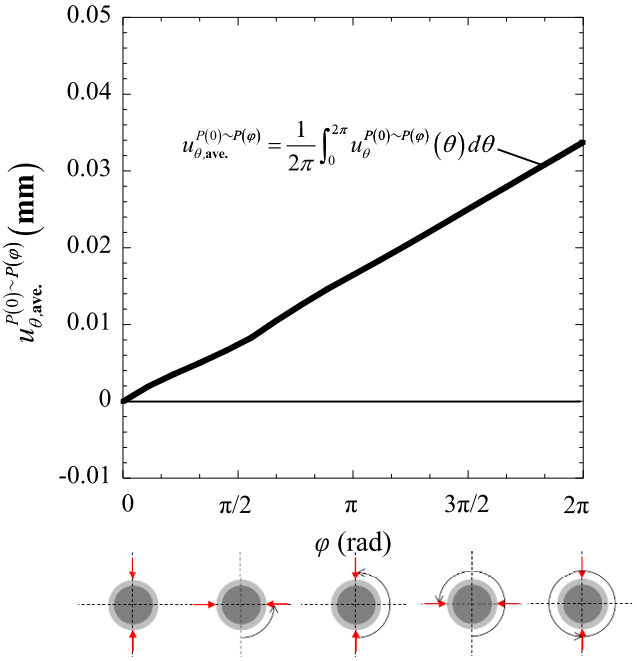

Fig. 7. History of average of displacement of the sleeve interface when P is shifted. (Online version in color.)

relative slippage condition.[4] Eventually, they have reported that the stress quasi-equilibrium region $\tau_{r\theta} \cong |\mu\sigma_r|$ at the shrink-fitted surface causes the residual deflection. In this research, the slippage in the circumferential direction is targeted, and the slippage direction differs from the study by Noda *et al.* (axial slippage). However, similar to the results of Noda *et al.*, the accumulation of the circumferential displacement in this study is considered to be related to interfacial slippage.

In this section, in order to confirm the existence of the circumferential residual displacement, firstly the slip region is examined, then the change of the residual displacement is examined. Therefore, by removing the loading the residual displacement will be discussed.

Figure 8 shows the shear stress distributions $\tau_{r\theta}^{P(0)}$, $\tau_{r\theta}^{P(0)\to 0}$ in comparison with the frictional stresses $\mu\sigma_r^{P(0)}$, $\mu\sigma_r^{P(0)\to 0}$ along the shrink-fitting surface. Figure 8(a) shows the results under the load $P(0)$ at $\varphi = 0$ and $\varphi = \pi$. Figure 8(b) shows the results after removing the load $P(0)$. The notation $P(0)$ denotes the pair of loads at $\varphi = 0$ and $\varphi = \pi$. The notation $P(0) \to 0$ denotes removing the load $P(0)$ after applying $P(0)$. In this study, the friction coefficient $\mu = 0.3$ is assumed between sleeve and shaft. By considering the FEM accuracy, the region satisfying $\tau_{r\theta} = \mu\sigma_\theta$ within the error ± 1 MPa is defined as the slippage region.

In Fig. 8(a), the slippage region $\tau_{r\theta}^{P(0)} \cong |\mu\sigma_r^{P(0)}|$ can be seen near the loaded position $\theta = 0$ and π. When the initial load $P(0)$ is applied, therefore, the slippage occurs around $\theta = 0$. As shown in Fig. 8(b), after removing the initial load as $P(0) \to 0$, the slippage region becomes smaller. However, the slippage region still can be seen near the loaded position $\theta = 0$ and π.

Next, to confirm the residual displacement, **Fig. 9** shows the displacement distributions under the initial load $P(0)$ and after removing the initial load as $P(0) \to 0$. From Fig. 9, it is confirmed that the displacement remains near the slippage region after removing the load. When the load is shifting, the residual displacement is accumulated and the average displacement increases with increasing the load shifting angle.

On the basis of the above simulation results, the interfacial creep generation can be confirmed experimentally in a real sleeve roll. In this experimental study, a four-stage compact rolling mill can be used without difficulty under the condition where the rotational torque effect can be neglected. After the simulation accuracy can be improved, for example, by replacing the rigid roll with an elastic roll, the experiment can be started. Also, in the further numerical simulation studies, the effects of the shaft torque T, the friction force S, the rolled material and the bearing force P_b in Fig. 3(a) can be discussed.

5. Conclusions

In this research, since few studies are available, numerical simulation was performed to realize the interface creep in

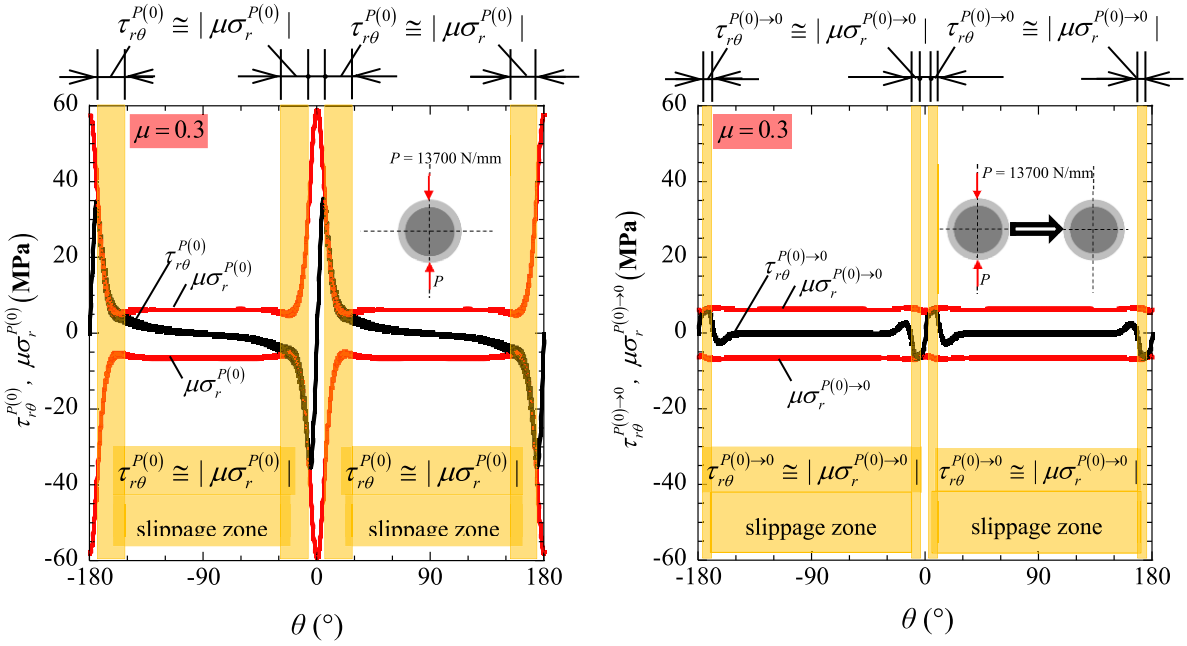

(a) Under the initial loading $P(0)$ (b) After removing the initial loading $P(0)$

Fig. 8. Comparison of slippage zone due to loading $P(0)$ and due to unloading $P(0) \rightarrow 0$. (Online version in color.)

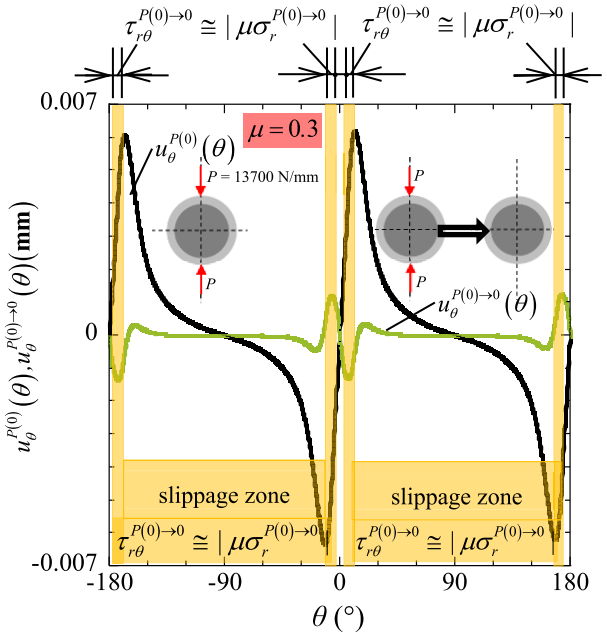

Fig. 9. Comparison between loading $u_\theta^{P(0)}(\theta)$ and unloading $u_\theta^{P(0)\rightarrow 0}(\theta)$. (Online version in color.)

a shrink-fitted sleeve roll used in a four-stage rolling mill. The conclusion can be summarized in the following way.

(1) The roll rotation is expressed by the load shifting on the fixed roll surface. The interfacial creep can be simulated by quasi-static FEM analysis in the roll.

(2) The skew-symmetry of the displacement $u_\theta^{P(0)}(\theta)$ caused by the initial load $P(0)$ disappears when the load is shifting as shown in $u_\theta^{P(0)\sim P(\pi)}(\theta)$ in Fig. 6(b). The symmetry condition is lost by the accumulation of the residual displacement at the interface due to the load shifting. As a result, the interfacial creep occurs.

(3) Although the magnitude of $u_\theta^{P(0)\sim P(\pi)}(\theta)$ varies depending on θ, the average displacement $u_{\theta,\mathbf{ave.}}^{P(0)\sim P(\varphi)}$ increases with increasing the load shift angle φ as shown in Fig. 7.

The slippage region is found from the stress distributions along the interface under the initial load and after the load is removed as shown in Fig. 8. The residual displacement along the interface is confirmed after the initial load is removed as shown in Fig. 9.

REFERENCES

1) H. Shimoda, S. Onodera, K. Hori and O. Dohi: *Trans. Jpn. Soc. Mech. Eng.*, **32** (1966), 689 (in Japanese).
2) H. Takigawa, K. Hashimoto, G. Konno and S. Uchida: *CAMP-ISIJ*, **16** (2003), 1150 (in Japanese).
3) T. Irie, K. Takaki, I. Tsutsunaga and Y. Sano: *Testu-to-Hagané*, **65** (1979), 293 (in Japanese).
4) N.-A. Noda, Y. Sano, Y. Takase, Y. Shimoda and G. Zhang: *J. Jpn. Soc. Technol. Plast.*, **58** (2017), 66 (in Japanese).
5) E. Matsunaga, Y. Sano and S. Nishida: *CAMP-ISIJ*, **10** (1997), 1078 (in Japanese).
6) E. Matsunaga, T. Tsuyuki and Y. Sano: *CAMP-ISIJ*, **11** (1998), 362 (in Japanese).
7) N. Soda: Bearing, Iwanami Shoten, Tokyo, (1964), 196.
8) T. Niwa: *NTN Tech. Rev.*, **81** (2013), 100.
9) J. Murata and T. Onizuka: *Koyo Eng. J.*, **166** (2004), 41.
10) Y. Sano: The 74th Technology of Plasticity Course, The Japan Society for Technology of Plasticity, Tokyo, (1999), 177.
11) N.-A. Noda, D. Suryadi, S. Kumasaki, Y. Sano and Y. Takase: *Eng. Fail. Anal.*, **57** (2015), 219.
12) N.-A. Noda, Y. Xu, D. Suryadi, Y. Sano and Y. Takase: *ISIJ Int.*, **56** (2016), 303.
13) T. Miyazaki, N.-A. Noda, F. Ren, Z. Wang, Y. Sano and K. Iida: *Int. J. Adhes. Adhes.*, **77** (2017), 118.
14) N.-A. Noda, T. Miyazaki, R. Li, T. Uchikoba, Y. Sano and Y. Takase: *Int. J. Adhes. Adhes.*, **61** (2015), 46.
15) N.-A. Noda, T. Uchikoba, M. Ueno, Y. Sano, K. Iida, Z. Wang and G. Wang: *ISIJ Int.*, **55** (2015), 2624.
16) Z. Wang, N.-A. Noda, M. Ueno and Y. Sano: *Steel Res. Int.*, **88** (2016), No. 7, http://doi.org/10.1002/srin.201600353.
17) N.-A. Noda, Y. Shen, R. Takaki, D. Akagi, T. Ikeda, Y. Sano and Y. Takase: *Theor. Appl. Fract. Mech.*, **90** (2017), 218.
18) N.-A. Noda, X. Chen, Y. Sano, M. A. Wahab, H. Maruyama, R. Fujisawa and Y. Takase: *Mater. Des.*, **96** (2016), 476.
19) Marc Mentat team: Theory and User Information, Vol. A, MSC. Software, Tokyo, (2008), 713.